Agricultural and Forest Meteorology 237 (2017) 71–79

Contents lists available at ScienceDirect

Agricultural and Forest Meteorology

journal homepage: www.elsevier.com/locate/agrformet

Impact of tree canopy on thermal and radiative microclimates in a mixed temperate forest: A new statistical method to analyse hourly temporal dynamics

Noémie Gaudio[a,*], Xavier Gendre[b], Marc Saudreau[c], Vincent Seigner[d], Philippe Balandier[d]

[a] INRA, UMR AGIR, 24 Chemin de Borde Rouge, CS 52627, F-31326 Castanet Tolosan Cedex, France
[b] IMT, UMR CNRS 5219,Université Paul-Sabatier, Route de Narbonne, F-31062 Toulouse Cedex, France
[c] INRA, UMR PIAF, 5 Chemin de Beaulieu, F-63039 Clermont-Ferrand Cedex 2, France
[d] IRSTEA, Unité de Recherche sur les Ecosystèmes Forestiers (EFNO), Domaine des Barres, F-45290 Nogent-sur-Vernisson, France

ARTICLE INFO

Article history:
Received 20 July 2016
Received in revised form
28 November 2016
Accepted 5 February 2017

Keywords:
Microclimate
Forest understorey
Temperature
Radiation
Principal component analysis

ABSTRACT

Forest shelter buffers microclimate, decreasing daily ranges of solar radiation and temperature, yielding higher minimum and lower maximum temperatures than those of open field. The most common way to analyse sets of these data is to compare mean, maximum and minimum values of climate parameters of open field and understorey conditions at daily, monthly or seasonal scales; however, this approach loses information about temporal dynamics. This study developed a statistical method to analyse hourly dynamics of temperature (T) and radiation (Rad) together and quantify effects of canopy openness and seasonality on these dynamics. Eight experimental sites were chosen in small gaps located in a temperate oak-pine forest (France), and five plots were established in each along a light gradient (i.e. a total of 40 plots), which delimited a transect along which T and Rad were measured hourly at a height of 200 cm from May 2009 to March 2010. T and Rad were also measured in open field. A specific Principal Component Analysis (PCA) with an innovative graphical representation was performed on this dataset. This statistical method allowed hourly temporal dynamics of all data recorded to be analysed and included a chart to interpret the distribution of the data in the principal plane defined by the PCA. Except in winter, results demonstrate the well-documented buffering effect of the tree canopy on T, with higher minimum and lower maximum values in the forest understorey. This effect was especially pronounced for minimum T and increased as canopy grew denser. In summer, T remained higher than expected in the understorey and was lower than expected in the open field, indicating thermal inertia in the understorey and an a priori cooling effect linked to wind or radiative losses during the night in the open field. The newly developed statistical method offers an innovative approach to better understand the tree canopy's buffering effect on temporal dynamics.

1. Introduction

In the current context of climate change, many concerns about the sustainability of ecosystems and crop production exist (Lobell and Gourdji, 2012), especially because temperatures are predicted to steadily increase in the near future and have a strong impact on many plant processes (Atkin et al., 2015; Blessing et al., 2015; Duursma et al., 2014; Kolari et al., 2014; Sendall et al., 2015). In forest ecosystems, understorey microclimate is controlled by characteristics (age, species, etc.) and the spatial structure of overstorey trees (Aussenac, 2000; Malcolm et al., 2001). Most microclimate variables are buffered by the shelter which trees provide (e.g. Karki and Goodman, 2015; Siegert and Levia, 2011; von Arx et al., 2012). Consequently, forest shelter creates cooler and wetter conditions for plant species sensitive to high temperatures or drought and thus thermophilisation of plant communities via macroclimate warming – i.e. favouring species adapted to warm conditions – could be limited (De Frenne et al., 2013). Therefore, both the macro- and microclimate should be considered to adequately predict the

* Corresponding author.
E-mail addresses: Noemie.Gaudio@inra.fr (N. Gaudio), Xavier.gendre@math.univ-toulouse.fr (X. Gendre), Marc.Saudreau@inra.fr (M. Saudreau), vincent.seigner@irstea.fr (V. Seigner), philippe.balandier@irstea.fr (P. Balandier).

http://dx.doi.org/10.1016/j.agrformet.2017.02.010
0168-1923/

future of ecosystems. Many researchers have demonstrated that mean climate change, especially average temperature, is probably not the best way to predict adverse consequences of climate change on ecosystems (Thornton et al., 2014) and Henttonen et al. (2014) emphasised the need to use high-resolution climate data when analysing tree growth.

Forest temperatures are often estimated from open field weather stations, sometimes located far from study sites, even though tree canopies modulate their own microclimate, and systematic differences between temperatures measured in forests and at open field weather stations have been identified (Kollas et al., 2014). As Körner (2016) emphasised, plants experience temperatures that are rarely reflected by average data and "to advance vegetation ecologists need to collect bioclimatic data, rather than rely on weather station data". Most ecological or physiological studies have used climate data at a resolution of several kilometres or more, whereas organisms experience microclimate at a finer scale, from millimetres to metres (Suggitt et al., 2011). While the general buffering effect of the tree canopy is known, i.e. a decrease in maximum temperatures and an increase in minimum temperatures, further investigation is needed into daily variations in temperature, and their relations to solar radiation below the canopy.

The buffered thermal range is influenced partly by reduced radiation in the understorey, as radiation and temperature are highly correlated (Bristow and Campbell, 1984; Jegede, 1997). Daily temperature and radiation dynamics are rarely considered together in studies linking understorey plant behaviour to microclimate characteristics, even though temperature alone is often not enough to explain plant processes. For example, phenology of leaf senescence is mainly under thermal control at low and middle latitudes, while photoperiod becomes the primary factor at high latitudes (Gill et al., 2015). Many studies address only radiation or temperature (often added to moisture). They mainly focus on i) impacts of these climate parameters on understorey plant behaviour (see e.g. Ammer (2003), Balandier et al. (2007) and Gaudio et al. (2011a,b) for light, and Butt et al. (2014) and De Frenne et al. (2013) for temperature) or ii) the microclimate itself, as modified by forest shelter (see e.g. Balandier et al. (2006b) for light and Morecroft et al. (1998) for temperature).

This study's aim was to accurately characterise microclimate in the forest understorey by considering both temperature and radiation, as they strongly influence plant processes. The dual challenge was to consider i) temperature and radiation together because the relation between the two could differ in the forest compared to the open field and ii) hourly dynamics of these two variables, to extend analysis beyond daily mean, minimum and maximum values. To this end, we used an exploratory method based on Principal Component Analysis (PCA) with an innovative graphical representation. This article focuses on describing the statistical method and its ability to describe forest microclimate defined by hourly dynamic behaviour of two or more climate parameters. In particular, it describes the buffering effect associated with forest shelter: conditions under which buffering occurs (i.e. the influence of canopy density or cover) and how seasonality influences it.

2. Materials and methods

2.1. Study site and experimental design

The study was conducted from May 2009 to March 2010 in the Orleans plain forest in France (47°51′–47°77′N, 2°25′–2°36′E, mean elevation: 140 m). This region has a semi-oceanic climate, with mean annual precipitation of 740 mm evenly distributed throughout the year and mean annual temperature of 11.3 °C (data from 1981 to 2010). In winter 2008, a network of eight experimental sites was established in mixed oak (*Quercus petraea* Lieblein) – Scots pine (*Pinus sylvestris* L.) stands (Table 1). Mean, minimum and maximum distances between the experimental sites were respectively 5.2, 1.2 and 11.2 km; therefore, they were considered independent. An open field site was also identified near the selected experimental sites to provide a reference measurement of the microclimate for all measurements described hereafter.

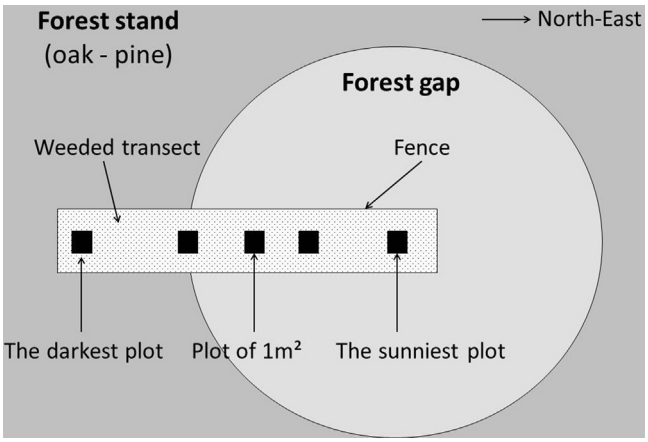

Fig. 1. Diagram of an experimental site (located in Orleans forest, France). Each experimental site consisted of one transect made up of five 1 m^2 plots organised to catch the light gradient at the stand – gap interface, i.e. the first plot was inside the forest stand (the darkest plot) and the fifth plot was in the middle of the gap (the lightest plot).

At each experimental site, we took advantage of small gaps (779 $m^2 \pm 352$ m^2) within the stand to increase the number of radiation situations explored. Each experimental site contained a transect with five 1 m^2 plots organised to capture the natural light gradient which occurs between a darker plot in the stand and a lighter plot in the middle of the gap (Fig. 1). As plot location was adapted to each stand's gap characteristics to capture the light gradient, the total length of transects ranged from 19 to 39 m, and the distance between two plots within a transect ranged from 3 to 25 m. The category "understorey conditions" grouped plots that were influenced by all degrees of tree canopy openness. All plots were kept free of understorey vegetation during the entire experiment. The experimental sites were fenced to protect them from wildlife.

2.2. Measurements

2.2.1. Temperature

In early spring 2009, experimental sites were equipped with temperature sensors, i.e. thermocouples (T type class 1, CETIB Dexis, Clermont-Ferrand, France), which measured temperature T with 0.01 °C precision. To measure air T instead of sensor T, each thermocouple was protected in a well-ventilated white shelter of 950 cm^3 to allow airflow. Data were recorded every minute, averaged at an hourly time step, and stored using a datalogger (CR800, Campbell Scientific Ltd, Loughborough, UK) powered by a 12 V battery. One thermocouple was placed at a height of 200 cm in each of the 40 plots (i.e. 8 sites × 5 plots). Another thermocouple was placed at a height of 200 cm in the open field to provide the reference T. Data were collected for eleven months, from May 2009 to March 2010.

2.2.2. Radiation

Incident quantum of Photosynthetic Active Radiation (PAR, 400–700 nm, μmol m^{-2} s^{-1}) was measured throughout the experiment (from May 2009 to March 2010) with a light sensor (DLT/BF3, Delta-T, Cambridge, UK) placed at a height of 200 cm in the open

Table 1
Forest stand characteristics for the eight experimental sites (S1,. . .,S8) sampled in mixed oak-Scots pine stands in the Orleans forest (France) within small gaps. Tree basal area ($m^2\ ha^{-1}$), number of stems (per ha), and mean height (m) were measured within a 20 m-radius of the darkest plot of the transect (Fig. 1), considering both dominant (overstorey) and dominated (understorey) tree strata. For the understorey, only trees higher than 2 m were considered.

	S1	S2	S3	S4	S5	S6	S7	S8
Overstorey								
Basal area	15.5	20.3	23.9	18.9	21.5	24.7	18.9	23.2
Number of stems	212	205	428	175	600	220	517	422
Height	23.0	21.1	22.8	19.9	16.3	25.2	20.0	18.4
Understorey								
Basal area	0.9	0.9	2.7	0.7	0.6	0.2	0.9	0.8
Number of stems	97	89	423	53	117	21	62	74
Height	12.3	8.4	8.9	7.7	7.4	9.5	7.5	8.6

field. Data were recorded every minute, averaged at an hourly time step, and stored using a datalogger (CR800, Campbell Scientific Ltd, Loughborough, UK) powered by a 12 V battery. PAR was also measured in all understorey plots, once in July 2009 (summer) with sensors and once in December 2009 (winter) with hemispherical photographs.

In July 2009, after light sensor calibration, PAR was measured at a height of 200 cm on each understorey plot using a light sensor (SKP 215, Skye Instruments, Llandrindod Wells, UK, $\mu mol\ m^{-2}\ s^{-1}$) connected to a datalogger (DataHog2, Skye Instruments, Llandrindod Wells, UK). Data were recorded every minute, averaged at an hourly time step, over a 24-h period. Transmitted PAR (PAR_t) in the understorey was then calculated as PAR measured in the forest divided by incident PAR (expressed as a percentage), thus eliminating the influence of differences in weather conditions on measurement days (Balandier et al., 2006a; Lieffers et al., 1999). PAR_t was considered a proxy of canopy openness.

In December 2009, canopy openness was estimated using one hemispherical photograph taken at a height of 200 cm in each plot, at sunrise or sunset. The equipment included a digital single lens reflex camera body (EOS-5D, Canon, Tokyo, Japan) with a circular fish-eye lens (8 mm F3.5 EX DG, Sigma, Kawasaki, Japan) with a 180° angle view. Then, photographs were thresholded in black and white using PiafPhotem software (Adam et al., 2006) to render pixels as vegetation (black) or sky (white). Finally, canopy openness (%) was calculated with Gap Light Analyzer software (http://ecostudies.org/gla/). Hemispherical photographs were also taken in July 2009 at a height of 200 cm to compare canopy openness estimated from hemispherical photographs to that measured by sensors; they were strongly correlated ($p < 0.0001$, $R^2 = 0.89$) (Gaudio, 2010).

Canopy openness calculations represented two contrasting forest canopy states: i) winter canopy openness, when oaks had no leaves, and ii) summer canopy openness, when oak foliage was fully developed. The short states of oak budding and leaf senescence are dynamic and intermediate between these two states, corresponding respectively to the first 15 days of May and November in French temperate forests (Balandier, 2014). For these two short sates, the two canopy openness values measured in summer and winter were averaged.

Radiation (Rad) in the understorey ($Rad_{understorey}$, $J\ m^{-2}\ s^{-1}$) was calculated at an hourly time step for each plot throughout the experiment based on the Rad measured in the open field ($Rad_{Openfield}$) and canopy openness (Eq. (1)):

$$Rad_{understorey}(J\ m^{-2}\ s^{-1}) = Rad_{Openfield}(\mu mol\ m^{-2}\ s^{-1}) \times 0.48 \times canopyopenness \quad (1)$$

where 0.48 is the conversion coefficient from $\mu mol\ s^{-1}\ m^{-2}$ to $J\ s^{-1}\ m^{-2}$ provided by the light-sensor supplier.

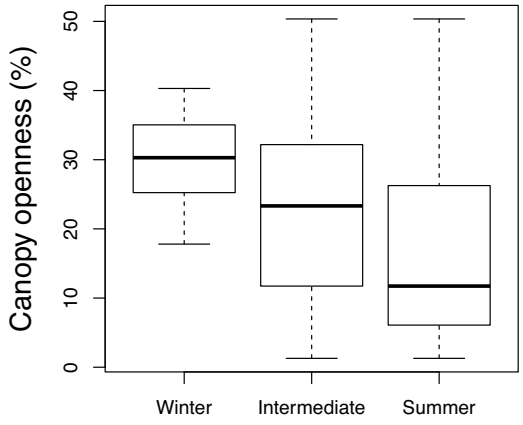

Fig. 2. Distribution of canopy openness (%) in mixed temperate oak-pine forest stand understorey (France). Canopy openness was considered in winter (December, January, February), intermediate months (May, September, October, November, March) and summer (June, July, August).

2.2.3. Microclimate during the experiment

Based on T measured in the open field, the experiment was divided into four periods (Table 2): winter (December, January, February), summer (June, July, August), intermediate warm (May, September) and intermediate cold (March, October, November). For most statistical analyses, the two intermediate periods were grouped into a single intermediate period.

Because understorey conditions consisted of multiple degrees of canopy openness, they can be considered as a single group or separated into different groups to capture the light gradient from the dense forest shelter to the forest gap. As the experiment was conducted in mixed oak-pine stands and oaks lost their leaves in winter, canopy openness in the open field and the understorey differed less in winter than in summer. For instance, canopy openness of the 25% most shaded plots in the understorey ranged from 17 to 25% in winter, 1–12% during the intermediate period and 1–6% in summer (Fig. 2).

2.3. Data analysis

Data were analysed using R software (http://www.r-project.org).

First, analyses of variance (ANOVAs) were performed to estimate T differences between the understorey (for all understorey plots) and the open field, considering daily mean (T_{mean}), maximum (T_{max}) and minimum (T_{min}) values for the entire experiment and the four seasonal periods. For these analyses, the canopy openness gradient in the understorey was ignored, as all understorey plots were grouped into a single "understorey" category. Regardless of the period considered, homogeneity of variance was systematically

Table 2
Mean, maximum (max) and minimum (min) air temperature (T, °C) and radiation (Rad, $J.m^{-2}.s^{-1}$) measured in open field conditions near the experimental sites (France) from May 2009 to March 2010. Months were grouped into four periods based on the temperature recorded: winter, intermediate cold, intermediate warm and summer.

Period	Month	T_{mean}	T_{max}	T_{min}	Rad_{mean}	Rad_{max}
Winter	December	3.7 ± 4.7	6.8 ± 4.6	−0.1 ± 4.9	65.1 ± 25.4	317.0 ± 143.5
	January	−0,1 ± 3.5	3.0 ± 3.7	−3.4 ± 4.2	35.0 ± 20.1	164.6 ± 104.0
	February	3.0 ± 5.1	6.8 ± 5.5	−0.6 ± 5.8	60.4 ± 29.3	263.8 ± 121.9
Intermediate cold	March	6.2 ± 4.9	12.3 ± 5.5	0.4 ± 5.6	123.7 ± 40.7	489.2 ± 125.4
	October	12.0 ± 3.8	18.8 ± 3.9	5.7 ± 5.2	90.3 ± 26.7	391.9 ± 102.3
	November	9.5 ± 3.1	13.0 ± 3.1	6.2 ± 3.5	45.5 ± 20.3	218.7 ± 93.7
Intermediate warm	May	14.3 ± 3.0	20.3 ± 4.0	7.1 ± 3.8	199.0 ± 82.9	631.1 ± 227.6
	September	14.6 ± 2.3	22.6 ± 3.7	7.9 ± 4.2	149.7 ± 51.0	537.8 ± 152.7
Summer	June	16.3 ± 3.0	22.3 ± 4.0	8.7 ± 3.3	237.3 ± 81.3	700.6 ± 218.5
	July	18.4 ± 2.5	24.8 ± 3.9	11.2 ± 3.1	229.5 ± 66.8	736.6 ± 168.0
	August	19.4 ± 2.4	28.0 ± 3.7	10.2 ± 3.2	225.5 ± 49.6	703.4 ± 129.9

verified using the Bartlett test. When relevant ($p < 0.05$), means were compared using the Tukey's HSD test.

Then, a PCA was performed and combined with an innovative graphical chart which interpreted results in the principal plane, with the originality of considering the shape of hourly (T, Rad) curves, with T and Rad considered simultaneously. Shapes of daily curves were compared to capture contrasting behaviour of 24-h (T, Rad) curves in the open field and the understorey, considering both the seasonal effect and the canopy openness gradient under the forest shelter. The statistical method developed in this study is a result itself (described in Sections 3.2 and 3.3), providing relevant perspectives and tools to analyse and understand sub-daily datasets, here composed of 8 experimental sites × 5 plots × 335 days × 24 h, with the additional open field site at the same time scale. The R code developed for the PCA is distributed according to the GNU GPL licence on the website of author Xavier Gendre (http://www.math.univ-toulouse.fr/~xgendre/rec/mtspca.tar.gz).

3. Results

3.1. Thermal differences between open field and understorey conditions

When considering the entire experiment, air T differences between open field and forest understorey (all understorey plots together, i.e. ignoring the understorey canopy openness gradient) were significant only for T_{min} (Table 3), with T_{min} higher in the understorey. Differences were more pronounced when considering seasonality of the data. T_{mean} was the same regardless of whether a forest shelter was present, even at the season scale, and no thermal variable distinguished open field from understorey in winter and intermediate cold period. T_{min} was significantly higher in the understorey than in the open field during warmer periods. Conversely, T_{max} was significantly lower in the understorey, but with less statistical significance. As a consequence, daily T were buffered in the understorey compared to the open field, especially T_{min}. This classic approach (ANOVA) helped to demonstrate well-documented thermal behaviours.

3.2. Relation between T and Rad between open field and forest understorey

It is well documented that seasonality and the presence of forest shelter influence air T and Rad, basically with higher T and Rad in summer and in open field than in winter and under forest shelter (Fig. 3). Spearman correlations were used to assess the relation between T and Rad. In open field, Spearman correlations were 0.80 and 0.73 between T and Rad for maximum and mean values, respectively. Correlations between minimum T and Rad values were not considered because they were assumed to occur at night, when solar radiation is absent (i.e. Rad is null regardless of environmental conditions). In understorey, Spearman correlations decreased to 0.25 and 0.29 between T and Rad for maximum and mean values, respectively. To identify interdependencies in such datasets, T and Rad should be considered together at a time scale finer than one day to characterise the microclimate of each plot for each day of the entire experiment. The method we developed focused on variations in hourly time-step curves around their daily means. Each observation consists of a pair of curves defined by the values measured (T, Rad) each hour (e.g. Fig. 4).

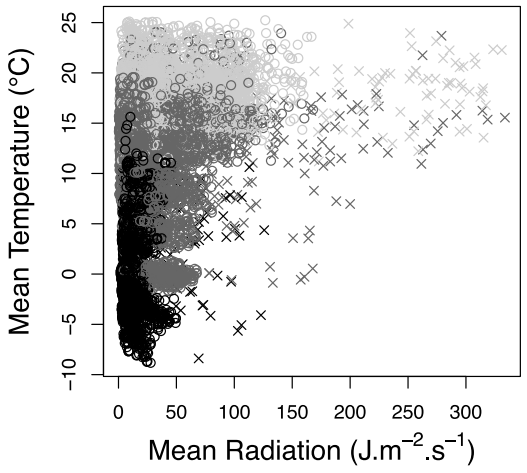

Fig. 3. Daily mean air temperature (°C) with respect to daily mean radiation ($J\,m^{-2}\,s^{-1}$) measured in mixed temperate oak-pine forest stand (understorey, o) and open field conditions (x) at 200 cm from May 2009 to March 2010. Black = winter (December, January, February), dark grey = intermediate months (May, September, October, November, March), light grey = summer (June, July, August).

3.3. Description of the statistical method

3.3.1. Data normalisation

For each pair of 24-h (T, Rad) curves, daily means $\bar{T}$ and $\overline{Rad}$ (Eq. (2)), and variances around these means σ_T^2 and σ_{Rad}^2, were calculated (Eq. (3)):

$$\bar{T} = \frac{1}{24}(T_1 + \cdots + T_{24})$$

$$\overline{Rad} = \frac{1}{24}(Rad_1 + \cdots + Rad_{24}) \quad (2)$$

$$\sigma_T^2 = \frac{1}{24}\sum_{h=1}^{24}\left(T_h - \bar{T}\right)^2$$

Table 3
Mean (T_{mean}), maximum (T_{max}) and minimum (T_{min}) air temperatures measured in mixed oak-Scots pine stands (understorey) and open field conditions from May 2009 to March 2010 (France). Data were considered at both whole-experiment and season scales, i.e. winter (January, February, December), intermediate cold (March, October, November), intermediate warm (May, September) and summer (June, July, August).

	Temperature	Openfield	Understorey	p-value
Whole experiment period	T_{mean}	10.4 ± 7.3	10.7 ± 7.4	NS
	T_{max}	15.9 ± 9.0	15.4 ± 8.8	NS
	T_{min}	4.6 ± 6.4	6.3 ± 6.8	<0.0001
Winter	T_{mean}	2.2 ± 4.7	2.1 ± 4.5	NS
	T_{max}	5.5 ± 4.9	5.1 ± 4.8	NS
	T_{min}	−1.4 ± 5.1	−1.2 ± 4.6	NS
Intermediate cold	T_{mean}	8.9 ± 4.6	8.8 ± 4.6	NS
	T_{max}	14.2 ± 5.1	13.5 ± 5.0	NS
	T_{min}	3.9 ± 5.5	4.6 ± 5.2	NS
Intermediate warm	T_{mean}	14.5 ± 2.7	14.8 ± 2.4	NS
	T_{max}	21.4 ± 4.0	20.2 ± 3.8	0.02
	T_{min}	7.5 ± 3.9	9.8 ± 3.1	<0.0001
Summer	T_{mean}	18.0 ± 2.9	18.2 ± 2.7	NS
	T_{max}	25.1 ± 4.6	24.1 ± 4.3	0.04
	T_{min}	9.9 ± 3.3	12.7 ± 2.8	<0.0001

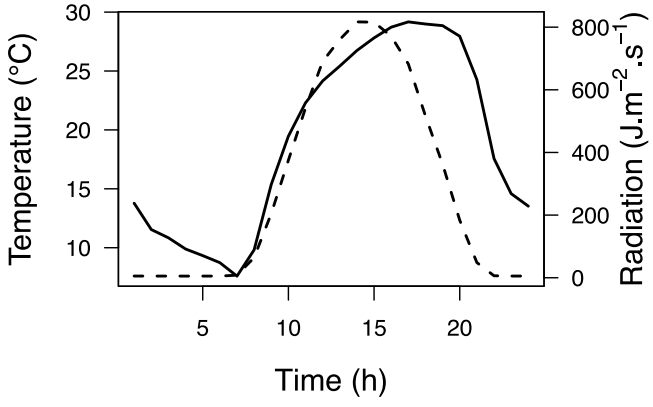

Fig. 4. Example of a pair of 24-h (temperature, radiation) curves measured on one plot at 200 cm in mixed temperate oak-pine forest stand on 12 August 2009 at an hourly time step. Dashed line = radiation (J m^{-2} s^{-1}), solid line = temperature (°C).

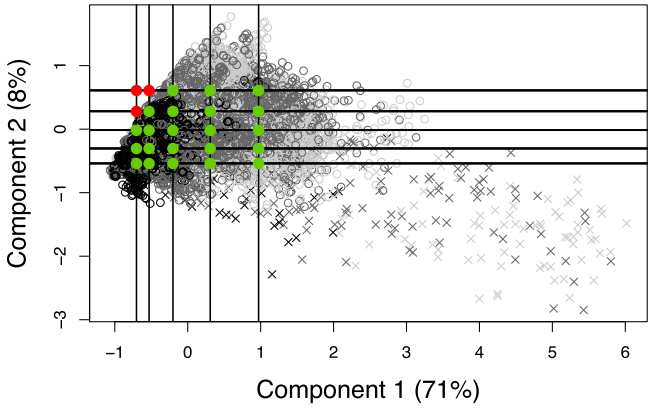

Fig. 5. Principal plane defined by the first two components of the Principal Component Analysis (PCA) performed on 24-h (temperature T, radiation Rad) curves measured in mixed temperate oak-pine stand understorey (o) and open field conditions (x) at 200 cm from May 2009 to March 2010. Components 1 and 2 explained respectively 71% and 8% of the data variability. Solid black lines refer to quantiles 0.1, 0.25, 0.5, 0.75 and 0.9. The ten nearest 24-h (T, Rad) curves from each quantile intersection were selected when their moment of inertia with respect to the quantile intersection was lower than 10% of the total inertia explained by the principal plane. Red points indicate 24-h (T, Rad) curves which were too far from the quantile intersection to be considered as representative, while green points indicate representative quantile intersections where means of the ten 24-h (T, Rad) curves were calculated for each intersection (see Fig. 8). Black = winter (December, January, February), dark grey = intermediate months (May, September, October, November, March), light grey = summer (June, July, August). (For interpretation of the references to color in this figure legend, the reader is referred to the web version of this article.)

$$\sigma^2_{Rad} = \frac{1}{24}\sum_{h=1}^{24}\left(Rad_h - \overline{Rad}\right)^2 \quad (3)$$

Next, the 24-h (T, Rad) curves were centred around their means, i.e. $\left(T - \bar{T}\right)$ and $\left(Rad - \overline{Rad}\right)$. Because the units of T and Rad have different scales, each curve (T, Rad) was normalised by dividing it by the respective mean of its variance (σ^2_T and σ^2_{Rad}) to preserve its range.

3.3.2. PCA procedure

Based on this normalised dataset, in which each observation provided two curves, each consisting of 24 variables (i.e. T and Rad at an hourly time step for 24 h) per plot per day, a PCA was performed to study the covariance structure of variations in T and Rad curves around their respective daily means (Ramsay and Silverman, 2005). Thus, each observation in the PCA consisted of 48 variables (T_1,. . .,T_{24}, Rad_1,. . .,Rad_{24}), yielding analysis of [335 days × 8 experimental sites × 5 plots] + [335 days × 1 open field site × 1 plot] = 13,735 observations. Of these observations, 11% were discarded due to temporary sensor failure, leaving 12,180 observations.

The two first principal components, C1 and C2, explained 79% of data variability (71% and 8%, respectively, Fig. 5). Coefficients of multiple correlation *r* (Keith, 2005) were calculated to measure the linear relation between each component and each climate parameter. The 24 variables for each of T and Rad were highly correlated with C1 (r = 0.76 for T and 0.96 for Rad) and C2 (r = 0.78 for T and 0.66 for Rad).

The large number of observations (i.e. 12,180) was divided into subsets to produce a synthetic representation of the entire dataset. The 24-h (T, Rad) curves belonging to the same subset were plotted together using a level set approach. Using a kernel density estimator (Baillo, 2003; Polonik, 1995), an envelope containing 75% of the observations in each subset was calculated to exclude outliers. Subsets were based on canopy openness (from 0 to 100%) in summer (Fig. 6), presence of a forest shelter (open field or forest understorey) and season (winter, intermediate period, summer) (Fig. 7).

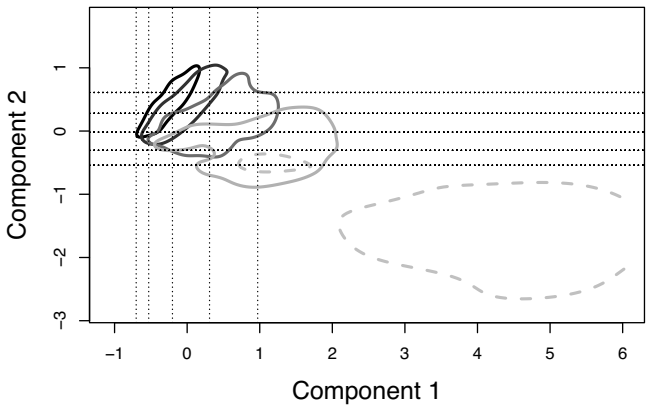

Fig. 6. Level sets in the principal plane containing 75% of the 24-h (temperature, radiation) curves in summer according to canopy openness. The grey dashed line represents open field. Solid lines represent understorey, which was classified according to four canopy openness quantiles ranging from 0 (black) to 1 (light grey) with a 0.25 step, i.e. Canopy openness (%) = [1–6],]6–12],]12–26], >26. Dotted lines represent the quantiles defined in Fig. 5.

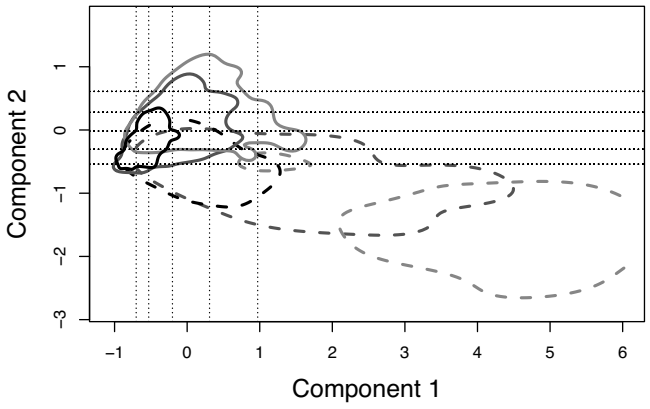

Fig. 7. Level sets in the principal plane containing 75% of the 24-h (temperature, radiation) curves in open field (dashed lines) and understorey conditions (solid lines) according to season (black = winter, dark grey = intermediate period, light grey = summer). Dotted lines represent the quantiles defined in Fig. 5.

Each subset had a different location in the principal plane, but it is not possible to interpret these differences without component-wise interpretation. Common approach to do so is based mainly on correlations between initial variables and principal components using the correlation circle method, in which arrow lengths and directions provide information about each variable (see e.g. Gomes et al. (2016)). Due to the large number of variables (i.e. 48) used to build the principal plane, this classic graphical representation of PCA was illegible, making it difficult to understand the principal plane. Therefore, a new graphical method using innovative read-out tools was developed to understand PCA axes and locations of observations in the principal plane.

3.3.3. Method for constructing a chart to interpret PCA axes

Each component of interest (C1 and C2) was a continuous variable that was discretely summarised by five quantiles (0.10, 0.25, 0.50, 0.75 and 0.90) to ensure sufficient representativeness of the sample along the component (Fig. 5). The two first components were then summarised by focusing on intersections of these quantiles. A second step provided representative 24-h (T, Rad) curves for each quantile intersection, following two precautionary measures:

- to smooth atypical 24-h (T, Rad) values (e.g. weather changes, short cloudy periods), the ten closest 24-h (T, Rad) curves of each quantile intersection were averaged instead of considering only the closest one,
- to avoid isolated quantile intersections (i.e. not representative of the dataset), the moment of inertia *I* of the ten closest 24-h (T, Rad) curves was calculated with respect to each quantile intersection. If *I* was higher than 10% of the inertia explained by the principal plane, the quantile intersection was considered isolated and was excluded from subsequent analyses (Fig. 5).

In this study's dataset, 22 quantile intersections were retained, each represented by the average of the ten closest 24-h (T, Rad) curves. These 22 averaged curves were kept to summarise distribution of observations in the principal plane, providing a chart to interpret the principal axes (Fig. 8). Each of the 22 cells in the chart illustrated the combined behaviour of the average T and Rad measurements representative of the 22 quantile intersections. One main advantage of the chart is a synthetic view of the dataset's spatial distribution in the principal plane, thus enabling easier interpretation.

3.4. PCA interpretation

Looking at the chart (Fig. 8) from left to right, component C1 showed a positive association between T and Rad, i.e. the higher the daily Rad range, the higher the daily T range, regardless of vertical location in the principal plane. Ranges of T and Rad were simultaneously lower on the left of the principal plane and higher on the right. Looking at the chart from bottom to top, component C2 showed opposite behaviour of T and Rad ranges. In a given column (i.e. horizontal location in the principal plane), high daily Rad ranges were associated with low daily T ranges at the bottom, and low daily Rad ranges were associated with high daily T ranges at the top. Information from the chart helps to interpret the locations of the observations in the principal plane.

In summer, when microclimate differences between open field and understorey were greatest (Table 3), the more the canopy was open, the more the associated subsets related to canopy openness moved from left to right along C1 (Fig. 6). Specifically, in the darkest understorey conditions, both Rad and T ranges were low, whereas as the forest canopy opened, Rad naturally increased, which increased the T range. Canopy openness subsets also showed a vertical gradient along C2 from the top for darkest conditions to the bottom for the lightest. These variations illustrate that T ranges in the understorey were higher than expected given the low Rad ranges. This was more evident as the canopy grew denser. Conversely, T ranges in sparse understorey and open field were smaller than expected given the high Rad ranges. This non-horizontal phenomenon was also observed when considering whether seasonality has the same impact on the relation between T and Rad in open field and in understorey (Fig. 7). In both open field and understorey conditions (all plots combined) the data subsets spread horizontally from winter to summer along C1, i.e. when the weather was warmer, Rad and T ranges increased regardless of the presence of a forest shelter. Along the vertical axis C2, the seasonal movement spread to the bottom for the open field and to the top for the understorey.

4. Discussion

As expected, regardless of season T_{mean} was statistically the same in the forest and open field. Körner (2016) demonstrated that T_{mean} eliminates the signal range that is integrated into the integrative variables T_{max} and T_{min}. This highlights the well-documented buffering effect of the forest canopy on daily T, with higher T_{min} and lower T_{max} in forest understorey than in open field (Ferrez et al.,

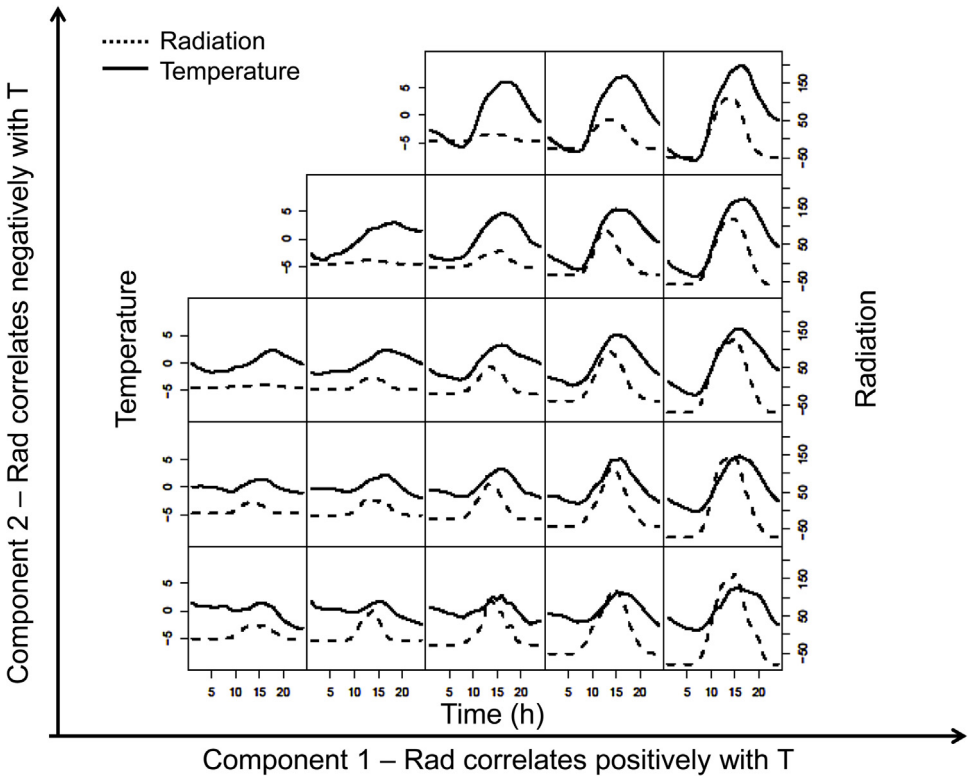

Fig. 8. Representative centred pairs of 24-h (temperature, radiation) curves (no meaningful unit) corresponding to the quantile intersections described in Fig. 5. Dotted line = radiation, solid line = temperature.

2011; Karki and Goodman, 2015; Morecroft et al., 1998). This effect occurred only during summer and the intermediate warm period. This is explained by the absence of oak foliage in winter, when open field and forest understorey have more similar conditions because less Rad is intercepted by the forest canopy. The buffering effect of forest canopy depends greatly on tree leaf area index (LAI). von Arx et al. (2013) identified an LAI threshold of 4 (sparse canopies), below which the buffering effect of temperate forest stands tend to disappear. The higher the T (i.e. in summer), the greater the effect of forest shelter (Renaud and Rebetez, 2009). This buffering effect was especially pronounced for T_{min} in our study. Renaud and Rebetez (2009) illustrated that, depending on the main tree species in the forest, the buffering effect can be higher for T_{min} (oak and pine) or T_{max} (beech, beech-silver fir, and oak-silver fir), due to differences in canopy closure.

Even though T and Rad are linked by definition, the relation between them was weakened under forest shelter, with Spearman correlations substantially lower in the understorey than in open field. Specifically, T can become high despite low Rad in understorey conditions, which suggests thermal inertia in the understorey (Jegede, 1997). For instance, daily T_{mean} can reach 25 °C at a daily Rad_{mean} of approximately 10 J m^{-2} s^{-1} in summer (Fig. 3). This highlights the need to include all climate parameters when studying microclimate. For instance, the presence of a forest shelter also decreases wind speed and buffers relative air humidity (Balandier and Prevosto, 2016; Renaud et al., 2011), which can influence T.

The previous results were obtained from classic statistical analysis (ANOVA) considering microclimate at the seasonal scale, i.e. pre-defined time divisions. Approaches using pre-defined time divisions, which cause a loss of information, have been applied at the seasonal scale (Renaud and Rebetez, 2009) and the daily scale (e.g. morning, afternoon) (Karki and Goodman, 2015). Although they provide information about microclimate behaviour, they depend greatly on weather conditions and seasonality and exclude information. Conversely, the method developed in this study makes no assumptions about time divisions, focusing instead on variations in hourly time-scale curves around their daily means, which thus includes all recorded data. The PCA procedure and the chart focused on 24-h (T, Rad) curves. The first component of the principal plane, C1, illustrated the well-documented buffering effect of tree canopy, with lower T and Rad ranges in dense understorey than in open field. The differences were greatest in summer and decreased when the canopy opened (Fig. 6). This confirmed the importance of considering microclimate variations in the understorey, with a buffering effect based on tree canopy structure and density. The value of our results is linked mainly to interpretation of the second component, C2. In forest understorey, when seasons became warmer, T was higher than expected assuming a linear relation between T and Rad. In understorey conditions, thermal inertia seemed to overcome the Rad effect, i.e. air T in forest stands decreased much more slowly in the afternoon on summer days than would be expected given the Rad alone. This is important to consider, especially for understorey vegetation and trees, which would experience greater thermal stress, and for a longer period, than assumed, even in shaded environments. However, extreme T was buffered in the understorey compared to the open field, particularly in summer. Based on these two points, a trade-off exists in the degree of canopy openness that ensures sufficient Rad for understorey vegetation and trees growth while also providing sufficient shelter to ensure the thermal buffering effect that may protect some species from climate change. Results demonstrated that even in shaded environments, T can remain high without high Rad, thus creating higher than expected thermal stress for understorey vegetation and trees. Conversely, T was lower than expected in the open field when seasons became warmer, suggesting that other parameters could have an influence. For example, during warm and sunny days, it is assumed that wind would buffer T. T_{min} can also decrease

relative to the heat lost from reflected longwave infrared energy during the night.

The R code developed for the PCA was written to consider 1 to n climate parameters together, e.g. air humidity and wind speed can be used to characterise forest microclimate if measurements are available. The method was designed for application to microclimate parameters measured at any time step (e.g. 1 min, 3 h).

5. Conclusion

The statistical method developed in this study adds substantive value to traditional analysis of a microclimate, especially because it can process all the data, whereas classic analyses usually begin by reducing the dataset (e.g. to mean, minimum and maximum values), which conceals several important features of microclimate dynamics. Thus, beyond than the demonstrated buffering effect of the canopy, the relation between temperature and radiation differed between forest understorey and open field conditions. Thermal inertia led to relatively high temperatures in more shaded conditions where canopy was dense and the opposite in more open conditions. Effects of other factors such as wind and nocturnal radiation losses decreased temperatures despite high radiation. Better understanding of forest microclimate behaviour could help improve predictions of future forest microclimates under climate change (Renaud et al., 2011). The method described in this article can help do this and would become more powerful if other climate parameters are included.

Acknowledgements

The authors thank Yann Dumas, Aurélien Brochet, Sandrine Perret, Michel Bonin and Florian Vast for their field assistance. This study was partly supported by a grant from the “Office National des Forêts”, France.

Appendix A. Supplementary data

Supplementary data associated with this article can be found, in the online version, at http://dx.doi.org/10.1016/j.agrformet.2017.02.010.

References

Adam, B., Benoit, J.C., Sinoquet, H., Balandier, P., Marquier, A., 2006. PiafPhotem – Software to Threshold Hemispherical Photographs. Version 1.0. UMR PIAF INRA-UBP (Clermont-Ferrand) – ALLIANCE VISION (Montélimar), France.

Ammer, C., 2003. Growth and biomass partitioning of *Fagus sylvatica* L. and *Quercus robur* L. seedlings in response to shading and small changes in the R/FR-ratio of radiation. Ann. For. Sci. 60, 9, http://dx.doi.org/10.1051/forest:2003009.

Atkin, O.K., Bloomfield, K.J., Reich, P.B., Tjoelker, M.G., Asner, G.P., Bonal, D., Boenisch, G., Bradford, M.G., Cernusak, L.A., Cosio, E.G., Creek, D., Crous, K.Y., Domingues, T.F., Dukes, J.S., Egerton, J.J.G., Evans, J.R., Farquhar, G.D., Fyllas, N.M., Gauthier, P.P.G., Gloor, E., Gimeno, T.E., Griffin, K.L., Guerrieri, R., Heskel, M.A., Huntingford, C., Ishida, F.Y., Kattge, J., Lambers, H., Liddell, M.J., Lloyd, J., Lusk, C.H., Martin, R.E., Maksimov, A.P., Maximov, T.C., Malhi, Y., Medlyn, B.E., Meir, P., Mercado, L.M., Mirotchnick, N., Ng, D., Niinemets, Ue., O'sullivan, O.S., Phillips, O.L., Poorter, L., Poot, P., Prentice, I.C., Salinas, N., Rowland, L.M., Ryan, M.G., Sitch, S., Slot, M., Smith, N.G., Turnbull, M.H., VanderWel, M.C., Valladares, F., Veneklaas, E.J., Weerasinghe, L.K., Wirth, C., Wright, I.J., Wythers, K.R., Xiang, J., Xiang, S., Zaragoza-Castells, J., 2015. Global variability in leaf respiration in relation to climate, plant functional types and leaf traits. New Phytol. 206, 614–636, http://dx.doi.org/10.1111/nph.13253.

Aussenac, G., 2000. Interactions between forest stands and microclimate: ecophysiological aspects and consequences for silviculture. Ann. For. Sci. 57, 15, http://dx.doi.org/10.1051/forest:2000119.

Baillo, A., 2003. Total error in a plug-in estimator of level sets. Stat. Probab. Lett. 65, 411–417, http://dx.doi.org/10.1016/j.spl.2003.08.007.

Balandier, P., Prevosto, B., 2016. Conséquences de l'application de sylvicultures dynamiques sur la biodiversité floristique du sous-bois en forêt: les apports d'un réseau d'expérimentation (Rapport Final De Projet). IRSTEA Nogent-sur-Vernisson, Convention MEDDE – DEB 2012–2015, pour la gestion des milieux et la biodiversité.

Balandier, P., Collet, C., Miller, J.H., Reynolds, P.E., Zedaker, S.M., 2006a. Designing forest vegetation management strategies based on the mechanisms and dynamics of crop tree competition by neighbouring vegetation. Forestry 79, 3–27, http://dx.doi.org/10.1093/forestry/cpi056.

Balandier, P., Sonohat, G., Sinoquet, H., Varlet-Grancher, C., Dumas, Y., 2006b. Characterisation, prediction and relationships between different wavebands of solar radiation transmitted in the understorey of even-aged oak (*Quercus petraea, Q-robur*) stands. Trees-Struct. Funct. 20, 363–370, http://dx.doi.org/10.1007/s00468-006-0049-3.

Balandier, P., Sinoquet, H., Frak, E., Giuliani, R., Vandame, M., Descamps, S., Coll, L., Adam, B., Prevosto, B., Curt, T., 2007. Six-year time course of light-use efficiency, carbon gain and growth of beech saplings (*Fagus sylvatica*) planted under a Scots pine (*Pinus sylvestris*) shelterwood. Tree Physiol. 27, 1073–1082.

Balandier, P., 2014. IMPREBIO: Impact de l'intensité des prélèvements forestiers sur la biodiversité – Impact of Wood Harvest Intensity on Forest Biodiversity (Final Report). IRSTEA Nogent-sur-Vernisson, MEDDE, GIP, Ecofor, INRA, Univ. Paul Cézanne, Univ. Rouen, ONF, France138.

Blessing, C.H., Werner, R.A., Siegwolf, R., Buchmann, N., 2015. Allocation dynamics of recently fixed carbon in beech saplings in response to increased temperatures and drought. Tree Physiol. 35, 585–598, http://dx.doi.org/10.1093/treephys/tpv024.

Bristow, K.L., Campbell, G.S., 1984. On the relationship between incoming solar radiation and daily maximum and minimum temperature. Agric. For. Meteorol. 31, 159–166, http://dx.doi.org/10.1016/0168-1923(84)90017-0.

Butt, N., Bebber, D.P., Riutta, T., Crockatt, M., Morecroft, M.D., Malhi, Y., 2014. Relationships between tree growth and weather extremes: spatial and interspecific comparisons in a temperate broadleaf forest. For. Ecol. Manag. 334, 209–216, http://dx.doi.org/10.1016/j.foreco.2014.09.006.

De Frenne, P., Rodriguez-Sanchez, F., Coomes, D.A., Baeten, L., Verstraeten, G., Vellend, M., Bernhardt-Roemermann, M., Brown, C.D., Brunet, J., Cornelis, J., Decocq, G.M., Dierschke, H., Eriksson, O., Gilliam, F.S., Hedl, R., Heinken, T., Hermy, M., Hommel, P., Jenkins, M.A., Kelly, D.L., Kirby, K.J., Mitchell, F.J.G., Naaf, T., Newman, M., Peterken, G., Petrik, P., Schultz, J., Sonnier, G., Van Calster, H., Waller, D.M., Walther, G.-R., White, P.S., Woods, K.D., Wulf, M., Graae, B.J., Verheyen, K., 2013. Microclimate moderates plant responses to macroclimate warming. Proc. Natl. Acad. Sci. U. S. A. 110, 18561–18565, http://dx.doi.org/10.1073/pnas.1311190110.

Duursma, R.A., Barton, C.V.M., Lin, Y.-S., Medlyn, B.E., Eamus, D., Tissue, D.T., Ellsworth, D.S., McMurtrie, R.E., 2014. The peaked response of transpiration rate to vapour pressure deficit in field conditions can be explained by the temperature optimum of photosynthesis. Agric. For. Meteorol. 189, 2–10, http://dx.doi.org/10.1016/j.agrformet.2013.12.007.

Ferrez, J., Davison, A.C., Rebetez, M., 2011. Extreme temperature analysis under forest cover compared to an open field. Agric. For. Meteorol. 151, 992–1001, http://dx.doi.org/10.1016/j.agrformet.2011.03.005.

Gaudio, N., Balandier, P., Dumas, Y., Ginisty, C., 2011a. Growth and morphology of three forest understorey species (Calluna vulgaris, Molinia caerulea and Pteridium aquilinum) according to light availability. For. Ecol. Manag. 261, 489–498, http://dx.doi.org/10.1016/j.foreco.2010.10.034.

Gaudio, N., Balandier, P., Perret, S., Ginisty, C., 2011b. Growth of understorey Scots pine (*Pinus sylvestris* L.) saplings in response to light in mixed temperate forest. Forestry 84, 187–195, http://dx.doi.org/10.1093/forestry/cpr005.

Gaudio, N., 2010. Interactions pour la lumière au sein d'un écosystème forestier entre les arbres adultes, les jeunes arbres et la végétation du sous-bois. Orléans University, France.

Gill, A.L., Gallinat, A.S., Sanders-DeMott, R., Rigden, A.J., Gianotti, D.J.S., Mantooth, J.A., Templer, P.H., 2015. Changes in autumn senescence in northern hemisphere deciduous trees: a meta-analysis of autumn phenology studies. Ann. Bot. 116, 875–888, http://dx.doi.org/10.1093/aob/mcv055.

Gomes, L., de, C., Cardoso, I.M., Mendonça, E., de, S., Fernandes, R.B.A., Lopes, V.S., Oliveira, T.S., 2016. Trees modify the dynamics of soil CO_2 efflux in coffee agroforestry systems. Agric. For. Meteorol. 224, 30–39, http://dx.doi.org/10.1016/j.agrformet.2016.05.001.

Henttonen, H.M., Makinen, H., Heiskanen, J., Peltoniemi, M., Lauren, A., Hordo, M., 2014. Response of radial increment variation of Scots pine to temperature, precipitation and soil water content along a latitudinal gradient across Finland and Estonia. Agric. For. Meteorol. 198, 294–308, http://dx.doi.org/10.1016/j.agrformet.2014.09.004.

Jegede, O.O., 1997. Diurnal variations of net radiation at a tropical station – Osu, Nigeria. Theor. Appl. Climatol. 58, 161–168, http://dx.doi.org/10.1007/BF00865016.

Körner, C., 2016. When it gets cold, plant size matters – a comment on tree line. J. Veg. Sci. 27, 6–7, http://dx.doi.org/10.1111/jvs.12366.

Karki, U., Goodman, M.S., 2015. Microclimatic differences between mature loblolly-pine silvopasture and open-pasture. Agrofor. Syst. 89, 319–325, http://dx.doi.org/10.1007/s10457-014-9768-4.

Keith, T.Z., 2005. Multiple Regression and Beyond, 1st ed. Pearson, Boston, Mass.

Kolari, P., Chan, T., Porcar-Castell, A., Back, J., Nikinmaa, E., Juurola, E., 2014. Field and controlled environment measurements show strong seasonal acclimation in photosynthesis and respiration potential in boreal Scots pine. Front. Plant Sci. 5, 717, http://dx.doi.org/10.3389/fpls.2014.00717.

Kollas, C., Randin, C.F., Vitasse, Y., Koerner, C., 2014. How accurately can minimum temperatures at the cold limits of tree species be extrapolated from weather station data? Agric. For. Meteorol. 184, 257–266, http://dx.doi.org/10.1016/j.agrformet.2013.10.001.

Lieffers, V.J., Messier, C., Stadt, K.J., Gendron, F., Comeau, P.G., 1999. Predicting and managing light in the understory of boreal forests. Can. J. For. Res. 29, 796–811, http://dx.doi.org/10.1139/cjfr-29-6-796.
Lobell, D.B., Gourdji, S.M., 2012. The influence of climate change on global crop productivity. Plant Physiol. 160, 1686–1697, http://dx.doi.org/10.1104/pp.112.208298.
Malcolm, D.C., Mason, W.L., Clarke, G.C., 2001. The transformation of conifer forests in Britain – regeneration, gap size and silvicultural systems. For. Ecol. Manag. 151, 7–23, http://dx.doi.org/10.1016/S0378-1127(00)00692-7.
Morecroft, M.D., Taylor, M.E., Oliver, H.R., 1998. Air and soil microclimates of deciduous woodland compared to an open site. Agric. For. Meteorol. 90, 141–156, http://dx.doi.org/10.1016/S0168-1923(97)00070-1.
Polonik, W., 1995. Measuring mass concentrations and estimating density contour clusters. Ann. Stat. 23, 855–881, http://dx.doi.org/10.1214/aos/1176324626.
Ramsay, J., Silverman, B., 2005. Functional Data Analysis. Springer Series in Statistics Springer-Verlag, New York, http://dx.doi.org/10.1007/b98888.
Renaud, V., Rebetez, M., 2009. Comparison between open-site and below-canopy climatic conditions in Switzerland during the exceptionally hot summer of 2003. Agric. For. Meteorol. 149, 873–880, http://dx.doi.org/10.1016/j.agrformet.2008.11.006.
Renaud, V., Innes, J.L., Dobbertin, M., Rebetez, M., 2011. Comparison between open-site and below-canopy climatic conditions in Switzerland for different types of forests over 10 years (1998–2007). Theor. Appl. Climatol. 105, 119–127, http://dx.doi.org/10.1007/s00704-010-0361-0.
Sendall, K.M., Reich, P.B., Zhao, C., Jihua, H., Wei, X., Stefanski, A., Rice, K., Rich, R.L., Montgomery, R.A., 2015. Acclimation of photosynthetic temperature optima of temperate and boreal tree species in response to experimental forest warming. Glob. Change Biol. 21, 1342–1357, http://dx.doi.org/10.1111/gcb.12781.
Siegert, C.M., Levia, D.F., 2011. Stomatal conductance and transpiration of co-occurring seedlings with varying shade tolerance. Trees-Struct. Funct. 25, 1091–1102, http://dx.doi.org/10.1007/s00468-011-0584-4.
Suggitt, A.J., Gillingham, P.K., Hill, J.K., Huntley, B., Kunin, W.E., Roy, D.B., Thomas, C.D., 2011. Habitat microclimates drive fine-scale variation in extreme temperatures. Oikos 120, 1–8, http://dx.doi.org/10.1111/j.1600-0706.2010.18270.x.
Thornton, P.K., Ericksen, P.J., Herrero, M., Challinor, A.J., 2014. Climate variability and vulnerability to climate change: a review. Glob. Change Biol. 20, 3313–3328, http://dx.doi.org/10.1111/gcb.12581.
von Arx, G., Dobbertin, M., Rebetez, M., 2012. Spatio-temporal effects of forest canopy on understory microclimate in a long-term experiment in Switzerland. Agric. For. Meteorol. 166, 144–155, http://dx.doi.org/10.1016/j.agrformet.2012.07.018.
von Arx, G., Pannatier, E.G., Thimonier, A., Rebetez, M., 2013. Microclimate in forests with varying leaf area index and soil moisture: potential implications for seedling establishment in a changing climate. J. Ecol. 101, 1201–1213, http://dx.doi.org/10.1111/1365-2745.12121.